SAND2002-3734C

Self-consistent, two-dimensional, magneto-hydrodynamic simulations of magnetically driven flyer plates

R. W. Lemke, M. D. Knudson, A. C. Robinson, T. A. Haill, K. W. Struve, J. R. Asay, and T. A. Mehlhorn

Sandia National Laboratories, Albuquerque, New Mexico 87185-1186

(Received

The intense magnetic field generated by the 20 megaampere Z machine at Sandia National Laboratories is being used as a pressure source for material science studies. An application we have studied in great detail involves using the intense magnetic field to accelerate flyer plates (small metal disks) to very high velocities (> 20 km/s) for use in shock loading experiments. We have used two-dimensional (2D) magneto-hydrodynamic (MHD) simulation to investigate the physics of accelerating flyer plates using multi-megabar magnetic drive pressures. A typical shock physics load is comprised of conducting electrodes that are highly compressible at multi-megabar pressures. Electrode deformation that occurs during the rise time of the current pulse causes significant inductance increase, which reduces the peak current (drive pressure) relative to a static geometry. This important dynamic effect is modeled self-consistently by driving the MHD simulation with an accurate circuit model of Z. Self-consistent, 2D, MHD simulations are able to produce and predict time resolved velocity interferometry measurements when the drive circuit includes models of current losses and short circuiting in Z. Simulation results elucidate the phenomena contributing to the flyer velocity history, and show that electrical and hydrodynamic optimization of the load are necessary to minimize effects of time varying inductance. We have identified paths to producing a flyer velocity of ~40 km/s and peak isentropic pressure of ~10 Mbar. Details of the modeling, the physics and comparisons with experiment are presented.

I. INTRODUCTION

The intense magnetic field generated by the Z machine [1] at Sandia National Laboratories is being used as a pressure source for material science studies [2-7]. The machine can deliver up to 20 megaamperes (MA) of current to a short-circuited load in 200 nanoseconds (ns), which generates a peak magnetic field in the megagauss (MG) range. An application we have studied in great detail involves using the intense magnetic field to accelerate flyer plates (small metal disks) to very high velocities [8] for use in shock loading experiments. The flyer plate is allowed to collide with a target, which generates a shock in the target material. Measurements of the flyer velocity and the shock speed in the material are used in conjunction with the Rankine-Hugoniot jump conditions [9] to obtain the density, pressure, and internal energy of the material. Flyer plates on Z have been accelerated to peak velocities of up to 28 km/s, and have been used in shock loading experiments to obtain state-of-the-art equation of state (EOS) data of deuterium for pressures up to 1 megabar (Mbar) [5, 6].

The characteristics of the shock generated in the target, in addition to the measurement error, are dependent on the condition of the flyer plate at impact, which in turn depends on the time history of the pressure drive. Indeed, the validity of the technique depends on the generation of a steady, planar shock in the material sample. This requires that the flyer impact surface be coplanar with the target surface. In addition, the flyer density behind the impact surface should be uniform over a distance that produces a steady shock for a duration that yields the desired measurement accuracy. The analysis is simplified considerably when the collision between flyer and target is symmetric (i.e. flyer and target materials identical), which requires that some fraction of the flyer remain at solid density at impact.

The flyer can become significantly deformed due to spatial nonuniformities in the magnetic

drive pressure. Deformation of the electrodes causes the load inductance to increase, thereby affecting the drive current. In addition, the flyer material is significantly modified by Joule heating associated with the accelerating magnetic field. At impact the flyer may be comprised of solid, liquid, boiling and plasma regions. Measurements yield the flyer velocity history, and provide information on the planarity of the flyer at impact, but often can not provide unambiguous information pertaining to the state of the flyer. The latter, in addition to many other unmeasurable quantities, can be obtained from accurate magnetohydrodynamic (MHD) simulations.

We present results from self-consistent, two-dimensional (2D) MHD simulations of shock loading experiments that accurately produce and predict measured flyer velocities, in addition to the amount of bowing in the flyer impact surface. The excellent agreement between simulated and measured quantities indicates that the flyer dynamics (including the state of the flyer) predicted by the calculations are physically realistic. Details of the modeling and comparisons with experiment are presented in the following section, and in the Appendix. Conclusions and requirements for optimizing shock physics loads to yield maximum drive pressure for a given current are discussed in Sec. III.

II. 2D MHD SIMULATIONS AND COMPARISON WITH EXPERIMENT

A 2D cross section of a typical flyer configuration (shock physics load) used on Z is shown schematically in Fig. 1 [5]. The actual geometry is three-dimensional (3D), with a similar cross section in the plane perpendicular to the figure. The magnetic pressure ($P_B=\mathbf{B}^2/2\mu_0$) initiates stress waves in the electrode material which compress the anode (A) and cathode (K). This causes the ak-gap [void (V) between anode and cathode] to increase. The flyer (F) moves independently of the surrounding anode without losing electrical contact after the initial stress wave releases from the front [target (T)] side of the flyer, and returns to the back (magnetic drive) side. The mag-

netic force (**JxB**) accelerates the flyer to peak velocity in approximately 0.3 cm, after which time it impacts the target.

Measurements and 3D electromagnetic simulation show that the magnetic field is uniform in the vertical direction of Fig. 1. Therefore, the problem geometry can be reduced to two dimensions without loss of generality. The relevant 2D cross section used in simulations is perpendicular to the plane of Fig. 1, which is indicated by the dashed line. The corresponding configuration used in 2D simulations is shown schematically in Fig. 2. The symmetry of the geometry permits simulations to be done using a quarter of the structure.

Two-dimensional Eulerian simulations were performed using the finite element, arbitrary Lagrangian-Eulerian, MHD code ALEGRA [10]. MHD equations for a compressible material (e.g., see [11]) with strength (e.g., see [12]) are solved. The yield strengths of materials used for electrodes (e.g., Al, Cu, W) are on the order of kilobars (Kbar). However, strength effects are not significant in this problem because the pressures involved are on the order of megabars (Mbar); that is, the material behavior is fluid-like. An EOS that is valid over a wide range of pressures, densities and temperatures is used [13], in addition to models for the thermal and electrical conductivities [14]. Density and internal energy are used in the EOS to obtain pressure and temperature. The density and temperature are used in the conductivity model to obtain electrical and thermal conductivities.

ALEGRA includes artificial viscosity, which broadens shock fronts. To ensure resolution of shocks, spatial cell sizes of 10-25 microns (μm) are used in the direction of flyer motion, and 20-50 μm in the transverse direction (the y- and x-directions, respectively, in Fig. 2). This resolution also ensures that energy is conserved to within a few percent.

Power flow into the shock physics load is affected by the dynamics of the electrodes caused

by the magnetic pressure. Deformation of the conductors, material motion and Joule heating increase the inductance and resistance of the load during the current pulse. Simulations must account for the coupling between machine and load in a self-consistent manner to accurately produce the drive current, which determines the time dependent flyer velocity. This is accomplished by coupling an accurate circuit model of the Z machine [15] to the geometry shown in Fig. 2. A generic model of the circuit is shown in Fig. 3. Power flows from the circuit into the 2D MHD simulation through the 3rd dimension of Fig. 2; that is, the direction of current flow is perpendicular to the plane of the figure. Although the simulation geometry is 2D, the coupling between MHD and circuit must account for the actual length of the load in the 3rd dimension so that the total inductance of the problem is calculated correctly. An outline of the coupling algorithm is provided in the Appendix, which also includes some details of the MHD used in ALEGRA.

The specific circuit was established by running simulations with different models and comparing results with measured currents and flyer velocities. The model that produced measurements most accurately includes a time dependent resistance (labeled R in Fig. 3) that emulates a short circuit in the machine; in addition to a nonlinear, time dependent model of current loss (labeled Z_{flow} in Fig. 3) that occurs upstream of the MHD load. These are plotted in Fig. 4(a), which also includes the time dependent machine voltage. The latter is an open circuit voltage derived using measurements of the forward traveling wave at the beginning of the magnetically insulated transmission line (MITL) that directs power to the load. The voltage across the loss impedance element [16] is given by $V_z = Z_{flow}\sqrt{I_u^2 - I_d^2}$, where I_u and I_d are currents upstream and downstream, respectively, of the location in the machine where the loss is thought to occur. This model implies a physical picture in which a short circuit occurs at the location of the current loss.

Values of the inductances L_c and L_{ext} (Fig. 3) are determined by the geometry of the MITLs. L_{ext} = 2.3 nanohenries (nH). L_c is split into two inductances, with 7.43 nH between the equivalent machine resistance (R_{eq} = 0.12 Ω) and short circuit switch (R), and 1.5 nH between R and Z_{flow}. The initial inductance of the MHD load is 2.7 nH, and is calculated self-consistently in the simulation using an effective transverse length of 3.6 cm.

Two-dimensional simulations of the geometry shown in Fig. 2 using the aforementioned circuit model produce currents like those shown in Fig. 4(b), which is a plot of I_u and I_d vs. time. The upstream and downstream currents would be identical without the loss impedance and short circuit switch. The decay time of the load current is determined by the total inductance in the circuit downstream of the short circuit, which includes the load inductance. The precise structure of the downstream (load) current waveform determines the time history of the flyer velocity.

Self-consistent, 2D, MHD simulations accurately produce and predict a variety of measured quantities including I_u and I_d, the time dependent flyer surface velocity [5], and interferometry measurements that determine the planarity of the flyer impact surface. Figure 5 is a comparison of measured and simulated flyer velocity and load current for the Fig. 2 geometry, in which an 850 μm Al flyer (density = 2.7 g/cm^3) is accelerated across a 0.33 cm long void where it impacts an Al target [5]. The simulated load current is within the measurement accuracy (~10%).

In experiments the velocity of the flyer surface closest to the target is measured [5]. This corresponds to the top surface of the flyer in Fig. 2. Figure 5 shows that the simulated flyer velocity is in excellent agreement with the measurement, the accuracy of which is on the order of 1%. Analysis of simulation results (details can be found in [17]) shows that the time dependent flyer velocity implicitly contains details pertaining to the current waveform, and other phenomena occurring within the flyer such as reverberations and Joule heating induced ablation. The latter

accounts for approximately 15% of the total velocity [17].

The initial step-up in flyer velocity [at 2.54 microseconds (μs) in Fig. 5] is due to the shocking up of the stress wave initiated by the magnetic drive pressure on the opposite side, and is proportional to the peak current. The shock must reflect from the surface in a way that keeps the total pressure equal to 0 (the void pressure). This generates a rarefaction (release) wave that propagates through the compressed material toward the back (drive side) of the flyer. When the release wave reaches the drive side a new stress wave whose magnitude is determined by the value of the magnetic field at that time is generated and propagates into the flyer. Thus, the initial pressure wave reverberates in the flyer. When the rise time of the current waveform is on the order of the round trip transit time for the initial compression and release waves, a reverberation of significant amplitude occurs resulting in a second step in velocity and recompression of the flyer. This is evident in the velocity histories shown in Fig. 5. Results show that a well defined and abrupt reverberation like that shown in Fig. 5 requires that the flyer have a region of solid density, which implies that the accelerating magnetic field has not diffused all the way through it [17].

The flyer becomes bowed in the plane of Fig. 2 due to spatial nonuniformities in the magnetic field. The magnetic field circulates around the cathode in Fig. 2 with x- and y-components. Consequently, the magnetic pressure decreases from the center of the anode-cathode gap (where it changes by less than 0.5% over the central 0.6 cm) out to the edge. Thus, the outer edge of the flyer moves slower than the center.

The planarity of the flyer is measured using time and space resolved interferometry to detect motion of the back surface of the target (top of Fig. 2). In simulations Lagrangian tracers that monitor material motion are placed at the corresponding location in the target, in a plane that is coplanar with the impact surface. If the flyer impact surface is coplanar with respect to the target

each tracer detects motion at the same time. If the flyer is bowed, tracers at the center of the impact plane detect motion before the outer tracers. A comparison of the simulated and measured bowing for the 850 μm flyer discussed above is shown qualitatively in Fig. 6, and quantitatively in Fig. 7.

In Fig. 6 a snapshot of the simulated shock physics load is compared with the time and space resolved interferometry image for target surfaces at 300 μm and 900 μm. The simulated image is at a time (~2.8 μs in Fig. 5) when the shock generated by the impact has reached a point 300 μm from the target surface. The simulated shock front is evidently curved. The curvature is reflected in the interferometry measurement which shows that points in the plane at 300 μm move later the farther they are from the center. This is shown quantitatively in Fig. 7, which compares the measured and simulated time that material motion occurs vs. distance from the center of the impact plane. The simulation accurately produces the measured bowing. Figure 7 shows that the shock front is planar over a diameter of ~1.5 mm, which allows jump conditions for planar shocks [9] to be used in the analysis of EOS measurements.

III. DISCUSSION AND CONCLUSIONS

The maximum flyer velocity that can be achieved for a given load configuration and drive current depends on the square of the peak magnetic field that is generated. The latter is determined by the peak current and geometry, which are coupled through the load inductance. Power flowing into the load is divided between magnetic, kinetic and internal energy. Significant conductor motion during the rise of the current pulse results in kinetic energy generation at the expense of magnetic energy, thereby reducing the peak magnetic pressure. Hence, producing the maximum pressure at the drive surface of the material sample (e.g., the flyer surface) requires: (1) a current waveform that minimizes electrode motion during the rise time, and (2) a geometry in

which magnetic flux is initially concentrated at the sample.

Magnetic flux at the sample is maximized by reducing alternative current paths in the load, which is accomplished by making the inductance of the current path that includes the sample much smaller than the inductances of all other paths [18]. Conductor motion during the current rise time is minimized by shaping the drive voltage waveform to produce isentropic compression; that is, the rise time of the voltage pulse is shaped so that the electrode materials are compressed along an isentrope of the EOS [18]. Self-consistent, 2D, circuit driven, MHD simulations of experiments designed for the refurbished Z machine [19] in which these ideas are incorporated predict isentropic compression of tungsten to a peak pressure of ~10 Mbar, and shockless acceleration of an aluminum flyer to a peak velocity of ~40 km/s [18].

Time resolved measurements of load current and flyer velocity taken in shock physics experiments on Z (exemplified by Fig. 5) were used to validate and improve physics models in the ALEGRA MHD code. This work led to improvements in the electrical conductivity model [14, 17], and determined possible models for machine dependent phenomena such as loss impedance and short circuiting. The resulting 2D, circuit driven, MHD model provides a fully self-consistent simulation that accurately produces and predicts time dependent shock physics measurements on Z. This provides evidence for the validity of the physics models used in ALEGRA, and implies that the ensemble of simulation results is realistic. Simulations of numerous flyer experiments have shown that the time dependent flyer velocity implicitly contains information pertaining to details of the drive current waveform, peak current, reverberations, state of the flyer, and the relative degree that ablation is affecting the velocity [17]. Thus, simulations that accurately produce measured quantities also yield physically realistic information pertaining to nonobservable quantities. This information has been useful for analyzing EOS measurements on Z, and for develop-

ing shock physics loads that yield higher drive pressures.

ACKNOWLEDGMENT

The authors thank Bryan Oliver of Mission Research Corporation for his insights pertaining to the circuit coupling problem. Sandia National Laboratories is a multi-program laboratory operated by Sandia Corporation, a Lockheed Martin Company, for the US Department of Energy under Contract DE-ACO4-94AL85000.

APPENDIX: MATHEMATICAL MODEL FOR COUPLING A CIRCUIT TO THE 2D MHD PROBLEM

The magnetic behavior of the dynamic shock physics load must be coupled self-consistently to the electrical behavior of the Z accelerator. This requires that a 2D, time-dependent partial differential equation describing the evolution of the magnetic field and current in the deforming conductors be solved simultaneously with a system of differential-algebraic equations describing the time-dependent lumped circuit model of the Z accelerator. The coupling must be accomplished so that the current and voltage characteristics as well as energy transfers computed by the mesh and circuit are equivalent. In this appendix we outline a robust and accurate coupling algorithm that was developed by one of the authors (A. C. Robinson).

We start with Maxwell's equations in the MHD limit, which assumes that the displacement current $\frac{\partial \vec{D}}{\partial t}$ is negligible. This requires a neutral plasma, $\rho_q = 0$, and $\nabla \cdot \vec{J} = 0$ where $\vec{J}$ is the current density. Then, Faraday's law, Ampere's law, and Ohm's law are respectively

$$\nabla \times \vec{E} = -\frac{\partial \vec{B}}{\partial t}, \qquad \nabla \times \frac{1}{\mu} \vec{B} = \vec{J}, \qquad \vec{J} = \sigma(\vec{E} + \vec{V} \times \vec{B}), \tag{1}$$

where σ is the electrical conductivity and μ is the permeability. These comprise three equations for three unknowns, $\vec{B}$, $\vec{J}$, and $\vec{E}$. The zero divergence law for $\vec{B}$ implies $\vec{B} = \nabla\times\vec{A}$. Substituting this into Faraday's law yields

$$\nabla\times\left(\vec{E} + \frac{\partial\vec{A}}{\partial t}\right) = 0 \quad \text{or} \quad \vec{E} = -\frac{\partial\vec{A}}{\partial t} - \nabla\phi. \tag{2}$$

Here $-\nabla\phi$ is an additive scalar potential representation for a portion of the electric field. For uniqueness we can specify the gauge condition $\nabla\cdot\vec{A} = 0$. The vector potential form of Faraday's law is combined with Ohm's law and Ampere's law to obtain,

$$\nabla\times\left(\frac{1}{\mu}\nabla\times\vec{A}\right) = \sigma\left(-\frac{\partial\vec{A}}{\partial t} - \nabla\phi + \vec{V}\times(\nabla\times\vec{A})\right) = \sigma\left(-\dot{\vec{A}} - \nabla\phi\right), \tag{3}$$

where the dot represents a total convective time derivative appropriate for a closed line integral. Boundary conditions on $\vec{A}$ and ϕ are required to specify the system.

Figure 8 is a schematic representation of the full 3D geometry. The shaded region represents the 2D plane of the MHD simulation with current in and out of the plane. The reduction of the 3D problem to an equivalent 2D problem with effective length L leaves A_z as the only non-zero vector potential component, which depends only on the x and y coordinates. Then $\partial\phi/\partial x = \partial\phi/\partial x = 0$ and $\partial\phi/\partial z = -E$ is constant in each disconnected region of non-zero σ. In the void region where $\sigma = 0$, $\phi = (\Phi(x,y) - \phi_0)\frac{z}{L} + \phi_0$ with $\Phi = \phi_K$ on $\partial\Omega_K$ and $\Phi = \phi_A$ on $\partial\Omega_A$, and Φ satisfies a 2D Laplacian (knowledge of Φ is not required). In the conducting regions

$$\sigma\left(\frac{dA_z}{dt} - E\right) = \sigma\left(\frac{\partial A_z}{\partial t} + V_x\frac{\partial A_z}{\partial x} + V_y\frac{\partial A_z}{\partial y} - E\right) = \frac{\partial}{\partial x}\left(\frac{1}{\mu}\frac{\partial A_z}{\partial x}\right) + \frac{\partial}{\partial y}\left(\frac{1}{\mu}\frac{\partial A_z}{\partial y}\right). \tag{4}$$

Boundary conditions on Γ_S imply zero normal gradients of A_z. In ALEGRA Eq. (4) is operator split into an "ideal" MHD step in which the nodes of the finite element mesh move at the material velocity while holding A_z constant on each node. This is followed by a diffusion solve on the new grid with the total derivative replaced by a partial derivative. Energy transfer with the external circuit happens only during the solution of

$$\sigma\left(\frac{\partial A_z}{\partial t} - E\right) = \frac{\partial}{\partial x}\left(\frac{1}{\mu}\frac{\partial A_z}{\partial x}\right) + \frac{\partial}{\partial y}\left(\frac{1}{\mu}\frac{\partial A_z}{\partial y}\right). \tag{5}$$

A circuit representation that accurately represents the response of this linear equation for the next time step is required. It will be used in a separate circuit solve to obtain the actual current flowing through the mesh.

The first step is to decompose the vector potential into two parts, $A_z = A_p + \hat{V}A_h$, where $\hat{V} = \phi_K - \phi_A$ is the unknown voltage drop across the mesh at the end of the time step. A_p is called the particular solution. Its initial condition for any given time step is the vector potential from the preceding time step and a zero voltage difference. A_h is called the homogeneous solution. Its initial condition is a zero vector potential with a unit voltage difference. The solution is thus parameterized by $\hat{V}$.

The simulations presented herein model both the anode and cathode conductors as well as the intervening void space. Each conducting region has its own value for E. The applied anode and cathode electric fields are $E_A = \frac{-(\phi_A - \phi_0)}{L}$ and $E_K = \frac{-(\phi_K - \phi_0)}{L}$. These scalar potential contributions represent the steady state solution. Current conservation between the anode and cathode steady state solutions, $E_K \int_{\Omega_K} \sigma d\Omega + E_A \int_{\Omega_A} \sigma d\Omega = 0$, is required since all the current in the cathode is required to return through the anode. Eliminating ϕ_0 from the previous three equations yields the following expressions for E_A and E_K,

$$E_A = \frac{(\phi_K - \phi_A)\int_{\Omega_K} \sigma d\Omega}{L\left(\int_{\Omega_A} \sigma d\Omega + \int_{\Omega_K} \sigma d\Omega\right)} \quad \text{and} \quad E_K = \frac{-(\phi_K - \phi_A)\int_{\Omega_A} \sigma d\Omega}{L\left(\int_{\Omega_A} \sigma d\Omega + \int_{\Omega_K} \sigma d\Omega\right)}, \tag{6}$$

which are proportional to $\hat{V}$.

Equation (5) is solved using linear finite elements and a backward Euler time integration for the particular and homogeneous solutions. Once this is accomplished an exact representation for the current can be recovered by integrating over the 2D volume of the anode (or cathode) to obtain a linear relation between current and voltage at the end of the time step. The result is

$$\hat{I} = \int_{\Omega_A} \sigma\left(\frac{\partial A_z}{\partial t} - E_A\right) d\Omega = a_1 + \hat{V} a_2 \quad , \tag{7}$$

where a_1 and a_2 are integral expressions involving the particular and homogenous solutions.

A response equation for the shock physics load on Z is required over the entire time interval. A conservation of energy principle is used to derive the necessary additional information. The magnetic energy conservation equation [which can be derived from Eq. (3)] is

$$\frac{d}{dt}\int_{\Omega}\left(\frac{B^2}{2\mu}\right) dV + \int_{\Omega} \sigma \vec{E} \bullet \vec{E} dV = -\int_{\Gamma} (\vec{E} \times \vec{H}) \cdot \vec{n} dS = VI. \tag{8}$$

Terms on the left-hand side of Eq. (8) represent the change in magnetic energy, and the Joule heating rate. There is no magnetic work term here because it occurs in the ideal MHD step before the diffusion solve. The right-hand side represents the Poynting flux through the boundary, which is equal to the power dissipated in the shock physics load (VI). The finite element formalism for solving the discrete equations permits the representation of this energy integral in a precise way.

The discrete volumetric energy changes can be exactly matched with the discrete Poynting flux integral, which can be shown to be equal to $\hat{V}\hat{I}\Delta t$. Combining this with Eq. (7) yields

$$\Delta t\left[-\frac{a_1}{a_2}\hat{I}+\frac{1}{a_2}\hat{I}^2\right] = \Delta t[b_1\hat{I}+b_2\hat{I}^2] = \int_0^{\Delta t}(VI)dt. \tag{9}$$

To ensure energy conservation, it is essential for the response function V to reflect both the current and the rate of change of current. Thus, we assume that the response function for the shock physics load can be represented as

$$V = L\dot{I}+RI, \tag{10}$$

where L and R are an effective inductance and resistance valid for one time step. Failure to represent the response in this way may result in energy mismatches between the circuit solver and the finite element solution. Insert $\hat{I} = I_0+\dot{I}_0\Delta t = I_0+\delta I$ in the discrete form on the left hand side of Eq. (9), and compute the energy using $I = I_0+\dot{I}_0 t$ and Eq. (10) in the integrand. Then assume $\delta I \ll I_0$, equate powers of δI, and compare equal order terms to obtain

$$R = \frac{b_1}{I_0}+b_2 \quad \text{and} \quad L = b_2\Delta t, \tag{11}$$

which is sufficient except at zero current crossing. This problem can be resolved by keeping the above definition of L, and defining R as follows

$$R = \frac{(b_1\hat{I}+b_2\hat{I}^2)-b_2\delta I(I_0+(\delta I)/2)}{(I_0^2+I_0(\delta I)+(\delta I)^2/3)}, \tag{12}$$

which has the proper limiting behavior for $\delta I \ll I_0$. Equation (12) is obtained by demanding that

energy be conserved exactly, and by assuming that $\dot{I}_0$ is constant throughout the interval. The value of $\dot{I}_0$ at the beginning of the interval is used for computing R.

Equations (10)-(12) are the circuit representation of the shock physics load in the ensemble of circuit equations. The circuit equation solver is integrated over a time interval Δt, which yields $\hat{V}$ at the end of the interval. Thus, $A_z = A_p + \hat{V}A_h$ solves the field equations and conserves energy exactly between the MHD mesh and circuit for linear current profiles. This algorithm is an accurate and robust procedure for solving 2D, flyer plate problems coupled to an external circuit.

REFERENCES

[1] R. B. Spielman, C. Deeney, G. A. Chandler, M. R. Douglas, D. L. Fehl, M. K. Matzen, D. H. McDaniel, T. J. Nash, J. L. Porter, T. W. L. Sanford, J. F. Seaman, W. A. Stygar, K. W. Struve, S. P. Breeze, J. S. McGurn, J. A. Torres, D. M. Zagar, T. L. Gilliland, D. O. Jobe, J. L. McKenney, R. C. Mock, M. Vargas, T. Wagoner, and D. L. Peterson, Phys. Plasmas **5**, 2105 (1998).

[2] J. R. Asay, in Shock Compression of Condensed Matter-1999, edited by M. D. Furnish, L. C. Chhabildas, and R. S. Hixson (AIP Press, New York, 2000), p. 261.

[3] C. A. Hall, J. R. Asay, M. D. Knudson, W. A. Stygar, R. B. Spielman, T. D. Pointon, D. B. Reisman, A. Toor, and R. C. Cauble, Rev. Sci. Instrum. **72**, 3587 (2001).

[4] D. B. Reisman, A. Toor, R. C. Cauble, C. A. Hall, J. R. Asay, M. D. Knudson, and M. D. Furnish, J. Appl. Phys. **89**, 1625 (2001).

[5] M. D. Knudson, D. L. Hanson, J. E. Bailey, C. A. Hall, J. R. Asay, and W. W. Anderson, Phys. Rev. Lett. **87**, 225501-1 (2001).

[6] M. D. Knudson, D. L. Hanson, J. E. Bailey, C. A. Hall, and J. R. Asay, submitted to Phys. Rev. Lett..

[7] R. P. Drake, Phys. Plasmas **9**, 3545 (2002).

[8] H. Knoepfel, *Pulsed High Magnetic Fields* (North Holland Publishing Company, London, 1970), pp. 116-122.

[9] A. V. Bushman, G. I. Kanel, A. L. Ni, and V. E. Fortov, *Intense Dynamic Loading of Condensed Matter* (Taylor and Francis, Washington, D. C., 1993), p. 6.

[10] R. M. Summers, J. S. Peery, M. W. Wong, E. S. Hertel, Jr., T. G. Trucano, and L. C. Chhabildas, Int. J. of Impact Engng. **20**, 779 (1997).

[11] L. D. Landau and E. M. Lifshitz, *Electrodynamics of Continuous Media* (Pergamon Press,

New York, 1960), pp. 213-217.

[12] A. V. Bushman, G. I. Kanel, A. L. Ni, and V. E. Fortov, *Intense Dynamic Loading of Condensed Matter* (Taylor and Francis, Washington, D. C., 1993), pp. 1-12 and pp. 34-46.

[13] G. I. Kerley, Kerley Publishing Services Report No. KPS98-1, 1998 (unpublished).

[14] M. P. Desjarlais, J. D. Kress, and L. A. Collins, Phys. Rev. E **66**, 025401(R) (2002).

[15] K. W. Struve, T. H. Martin, R. B. Spielman, W. A. Stygar, P. A. Corcoran, and J. W. Douglas, Digest of Technical Papers, 11th IEEE Int. Pulsed Power Conf., ed. by G. Cooperstein and I. Vitkovvitsky, Baltimore, MD, p. 162 (1997).

[16] C. Mendel and S. E. Rosenthal, Phys. Plasmas, Vol. 2, No. 4, p. 1332 (1995).

[17] R. W. Lemke, M. D. Knudson, C. A. Hall, T. A. Haill, M. P. Desjarlais, J. R. Asay, and T. A. Mehlhorn, submitted to Phys. Plasmas.

[18] R. W. Lemke, A. C. Robinson, M. D. Knudson, T. A. Haill, K. W. Struve, J. R. Asay, and T. A. Mehlhorn, *Proceedings of the International Conference on High-Power Particle Beams and Dense Z-Pinches*, Albuquerque, NM, June 2002.

[19] M. G. Mazarakis, D. H. McDaniel, E. A. Weinbrecht, K. W. Struve, J. E. Maenchen, W. A. Styger, D. L. Johnson, and J. P. Corley, *Proceedings of the International Conference on High-Power Particle Beams and Dense Z-Pinches*, Albuquerque, NM, June 2002.

FIGURE CAPTIONS

FIG. 1. Cross section of 3D flyer configuration used in shock loading experiments. Anode (A) and cathode (K) are attached in a short circuit at the top of the figure. The flyer (F) is formed by boring out anode material to obtain a desired thickness. The flyer is accelerated across the void (V) and impacts a target (T). The directions of the surface current density (**J**) and magnetic field (**B**) are indicated by arrows. The region simulated is a 2D cross section perpendicular to the plane of the figure, which is indicated by the dashed line.

FIG. 2. Schematic of symmetric slab configuration used in 2D, circuit driven, MHD simulations. K=cathode=red, A=anode=green, F=flyer, T=target, V=void=black. There are two flyers, which are also part of the anode. The direction of current flow is perpendicular to the figure. The magnetic field generated by the cathode current fills the void region between cathode and anode, and has x- and y-components. The magnetic pressure accelerates the flyers in the vertical direction toward the target. Problem dimensions are: (1) cathode width and height are respectively 1.1 cm and 0.4 cm, (2) vacuum gaps between anode and cathode = 0.2 cm, (3) flyer thickness = 0.085 cm, and (4) height of void region through which flyer is accelerated is 0.33 cm.

FIG. 3. Equivalent circuit model of the Z machine used to drive 2D MHD simulations of shock physics loads. The load impedance for the circuit is the MHD simulation [see Eq. (10) in the Appendix]. V(t) = time dependent open circuit voltage, R_{eq} = equivalent machine resistance, L_c = MITL inductance, Z_{flow} = time dependent flow impedance current loss element, V_z = voltage across Z_{flow}, L_{ext} = inner MITL inductance, I_u = current upstream of Z_{flow}, I_d = current downstream of Z_{flow}, and R = time dependent resistive switch that emulates a short circuit. In simulations a fraction of L_c is placed upstream of R.

FIG. 4. (a) Time dependent open circuit voltage used to drive 2D MHD simulations. Also plotted

in the figure are the short circuit switch resistance (crowbar impedance), which has been scaled by 0.01, and the flow impedance (Z_{flow}) scaled by 1.71. (b) Simulated currents upstream (I_u = mitl) and downstream (I_d = load) of Z_{flow}. Without the loss element $I_u = I_d$. The precise shape of the I_d waveform is needed to produce and predict the measured time dependent flyer velocity.

FIG. 5. Comparison of simulated (red curves) and measured (black curves) flyer velocity (solid lines) and load currents (dashed lines) for an 850 μm Al flyer plate in the configuration shown in Fig. 2. The abrupt step in velocity at 2.54 μs is caused by a shock that reaches the front surface of the flyer. The sudden drop in flyer velocity at 2.76 μs marks the instant when the flyer collides with the target. In the experiment the flyer is wider than the target. The measurement does not show the collision event because it is taken from a point on the flyer that is outside of the target dimension.

FIG. 6. (a) Snapshot of material density from simulation of Fig. 2 geometry at a time after the front surface of the Al flyer (F) has collided with the Al target (T). The configuration is shown in quarter-symmetry. Full symmetry is obtained by reflecting the figure about the x- and y-axes. The cathode is denoted by K. The collision generates a shock in the target, the front of which is marked in the figure. The shock front is evidently curved, which is caused by a drive pressure that decreases with increasing x. The target material remains stationary until the shock front arrives. Measuring the time at which material begins to move in a horizontal plane at a given location is used to determine the exact curvature of the flyer at impact. (b) Time and space resolved laser interferometry measurement that detects motion in target surfaces located 300 μm and 900 μm from the impact surface. The result for 300 μm is enclosed by the dashed rectangle, which corresponds to the location of the shock front in (a). The right-hand boundary of the rectangle (i.e., the horizontal center of the figure) corresponds to x=0 in (a). The fringes are steady until the shock

arrives, after which time the reflectivity of the surface drops and the image turns black. The image shows that material motion occurs later with increasing distance from the impact center, which requires that the flyer be bowed as shown in (a).

FIG. 7. Comparison of the simulated and measured time of material motion vs. distance from the center of a horizontal plane located at y=300 μm from the impact surface [see Fig. 6(a)] in the target. The excellent agreement between the simulated and measured results indicates that the flyer bowing and resulting shock front in the target are as shown in Fig. 6(a). The data show that the shock front is planar over a central diameter of ~1.5 mm, which allows analysis of EOS measurements using jump conditions for planar shocks.

FIG. 8. 3D schematic of the problem domain. Although the geometry shown is cylindrical, the mathematical analysis applies to a general 2D Cartesian geometry with disjoint conducting regions. The shaded regions and the void space between them comprise the 2D simulation domain. The outer and inner regions are the anode and cathode, respectively, which are connected with a common potential ϕ_0 (i.e., short circuited) at the top of the figure. Current is assumed to enter through Ω_K at potential ϕ_K, and return through Ω_A at potential ϕ_A. On the vertical sides (Γ_S), $\frac{1}{\mu}\nabla\times\vec{A}\times\hat{n} = 0$ and $\vec{J}\cdot\hat{n} = 0$. On the top and bottom surfaces (Γ_A and Γ_K, respectively) $\vec{A}\times\hat{n} = 0$ with spatially constant values of ϕ_K, ϕ_A and ϕ_0. Poynting energy enters and leaves the system through the Γ_V surfaces where $\vec{A}\times\hat{n} = 0$ and $\vec{J}\cdot\hat{n} = 0$. The actual length, *L*, of the 3D configuration is used in the 2D simulation to ensure that the voltage and inductance are calculated accurately.

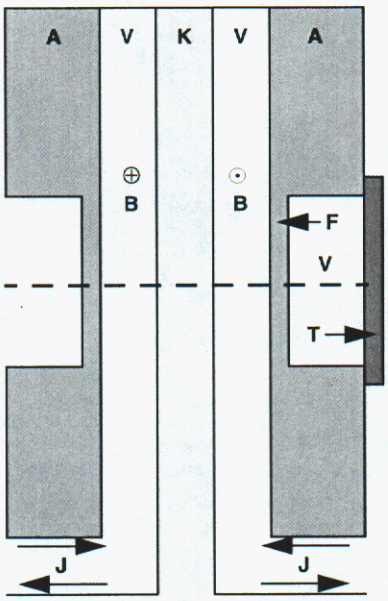

Figure 1, R. W. Lemke, Physics of Plasmas

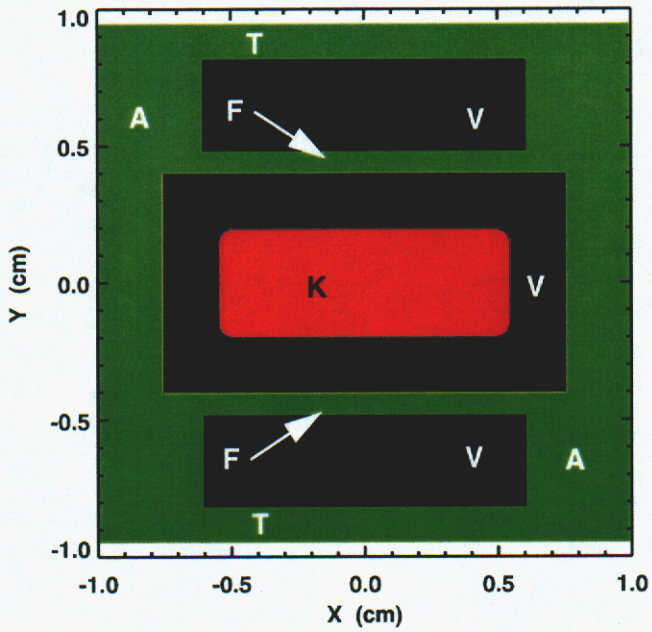

Figure 2, R. W. Lemke, Physics of Plasmas

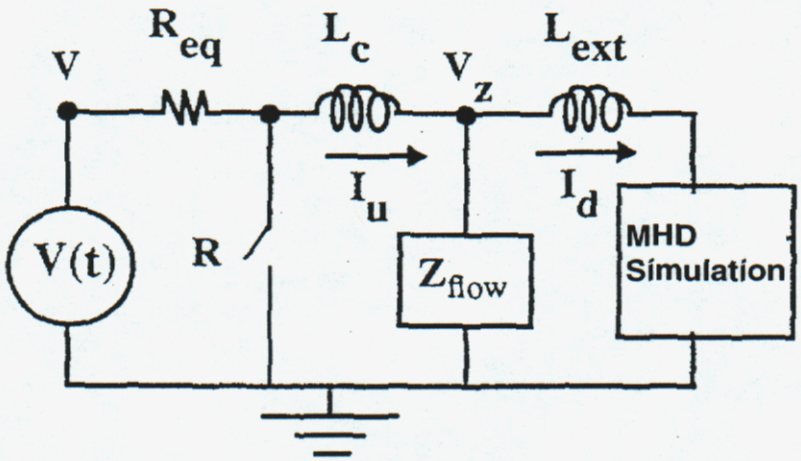

Figure 3, R. W. Lemke, Physics of Plasmas

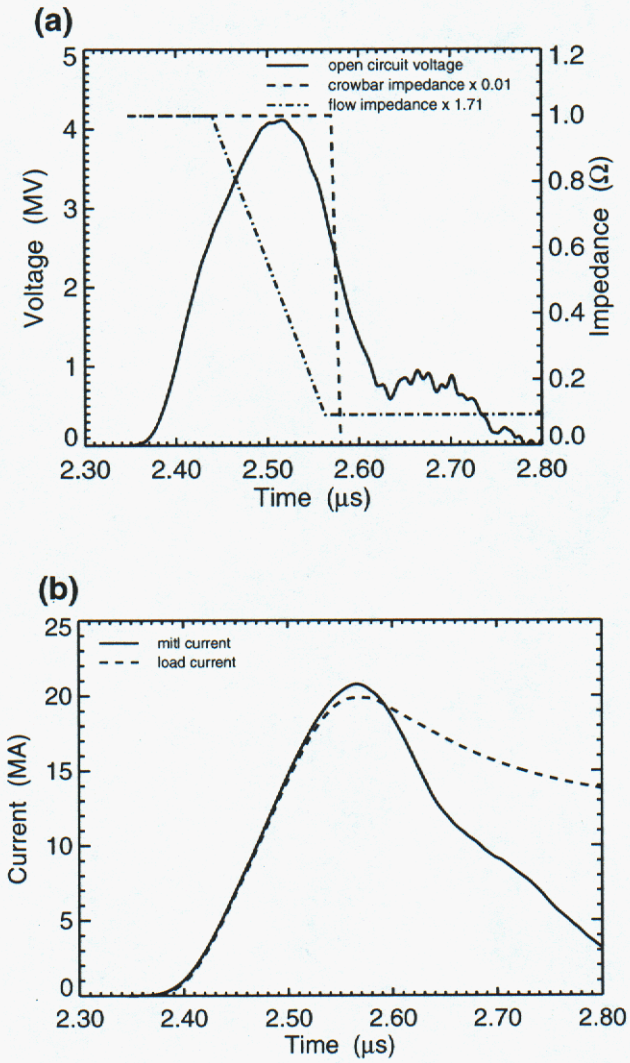

Figure 4, R. W. Lemke, Physics of Plasmas

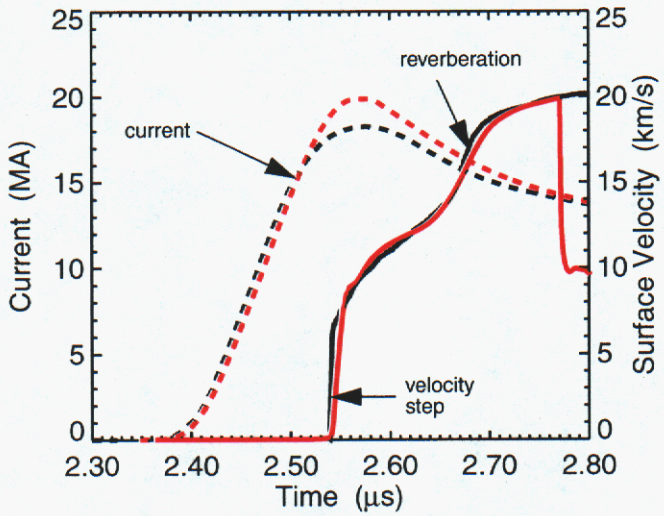

Figure 5, R. W. Lemke, Physics of Plasmas

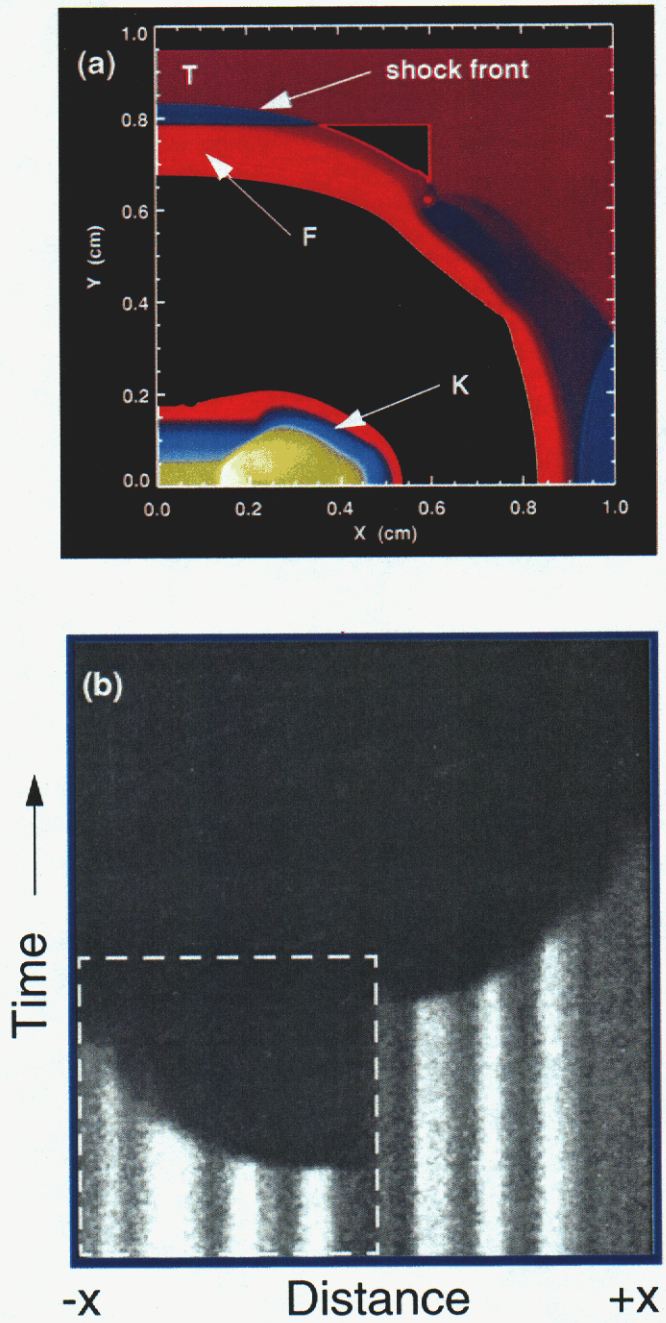

Figure 6, R. W. Lemke, Physics of Plasmas

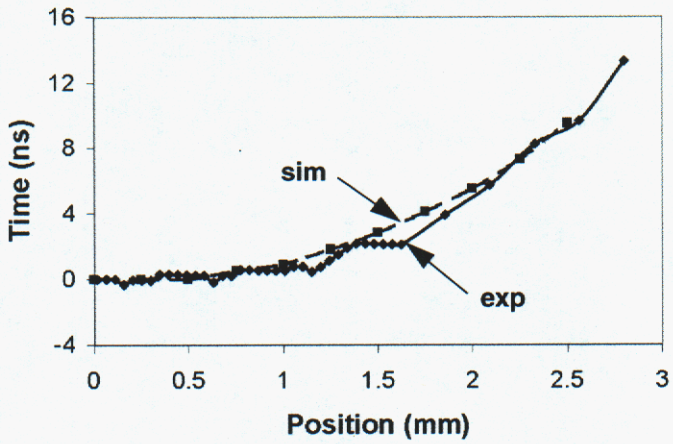

Figure 7, R. W. Lemke, Physics of Plasmas

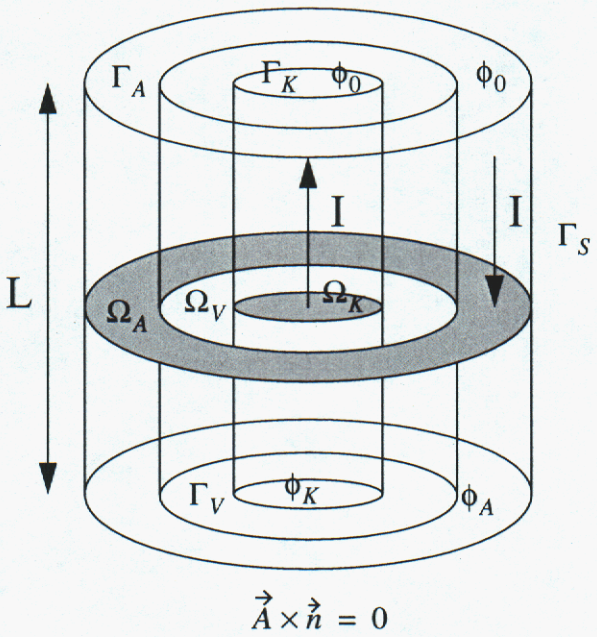

Figure 8, R. W. Lemke, Physics of Plasmas